

Influence of Carbon Chain Length on Biodiesel Combustion in an Optically Accessible Diesel Engine

R. Zhang¹, P.X. Pham², S. Kook¹ and A.R. Masri²

¹School of Mechanical and Manufacturing Engineering
The University of New South Wales, Sydney, NSW 2052, Australia

²School of Aerospace, Mechanical and Mechatronic Engineering
The University of Sydney, Sydney, NSW 2006, Australia

Abstract

This study focuses on laser-based imaging diagnostics of hydroxyl and soot during biodiesel combustion in a light-duty optical diesel engine. Planar laser-induced fluorescence of OH (OH-PLIF) and laser-induced incandescence (PLII) diagnostics were performed for two biodiesel fuels with different carbon chain lengths. The results show that longer carbon chain length leads to decreased ignition delay, which makes OH start to form closer to the bowl wall during the premixed combustion phase. For both fuels, soot formation starts to occur near the fuel-rich jet-wall impingement region at the end of the premixed combustion phase. However, it is only the longer carbon-chain biodiesel that shows additional soot formation in the penetrating wall-jet head region and overall higher amounts of in-cylinder soot.

Introduction

Studies have consistently shown that replacing petroleum diesel with biodiesel or its blends achieves a significant reduction in unburned hydrocarbons (uHC), carbon monoxide (CO) and particulate matter (PM) emissions [1]. It is understood that oxygen in biodiesel and the lack of aromatic contents are the main contributors for the reduced emissions [2]. However, the engine performance and emissions output for biodiesel depend strongly on the fuel molecular structures [3, 4]. The carbon chain length of fatty acid methyl (or ethyl) esters is one of the defining structural features of biodiesel, which represents the number of carbon atoms presented in the alkyl group. Saponification number is empirically used to measure the average carbon chain length of biodiesel with higher value representing shorter carbon chain length. Previous studies reported increased cetane number (i.e. ignition quality) and reduced oxygen concentration for lower saponification number (i.e. longer carbon chain) biodiesel [3], which resulted in higher PM but lower nitrogen oxide (NO_x) emissions [3, 4].

The current study aims to provide further insight into the effect of biodiesel carbon chain length on engine combustion by visualising the development of hydroxyl radical (OH) and soot inside the cylinder of the engine. Planar laser-induced fluorescence of OH (OH-PLIF) and laser-induced incandescence (PLII) were performed in a light-duty optical diesel engine. The laser diagnostics were repeated for two selected biodiesel surrogate fuels with different saponification numbers. Obtained laser images were supported by line-of-sight integrated images of electronically excited OH (OH*) chemiluminescence.

Experiments

Engine Specifications, Operating Conditions, and Fuel Properties

Specifications of the used engine are listed in table 1. The single-cylinder diesel engine has a displacement volume of 497.5 cm³ with 83 mm bore and 92 mm stroke. The piston has a quartz bowl window with flat surface that provides a non-distorted bottom view of the

piston bowl region. A 35-mm-wide section of the bowl rim was removed to provide access for the laser sheet to enter the bowl region. This has led to a geometric compression ratio of approximately 15.5. This bowl-rim cut-out however did not alter the in-cylinder swirl flow as proven by our full-cycle modelling study [5]. More importantly, the flame development occurs on the opposite side of the bowl wall and the diagnostics stopped before the flame reaches this cut-out region. The wall temperature was controlled by circling 363-K heated water through the cylinder liner, head and engine block. The engine is naturally aspirated and has a fixed swirl ratio of 1.4. The intake air temperature was measured to be at 303 K consistently throughout the experiments. The engine speed was maintained at 1200 rpm using an electric motor. The fuel injection system consists of a common-rail and a solenoid injector with a single-hole nozzle. This single-hole configuration allowed longer injection duration while keeping the in-cylinder pressure below the quartz window burst limit. The engine was operated under a 10-cycle skip-firing mode (i.e. one firing cycle every 10th motoring cycle) to further reduce thermal load on quartz windows and to expel residual gases from previous firing cycles. Schematic depiction of the used engine setup is illustrated in figure 1(a). More detailed descriptions of the figure are presented in the following sections.

The biodiesel compositions, main properties and corresponding injection conditions of tested fuels are listed in table 2. The fuels (labelled as C810 and C1214) have similar iodine values (1 and 8), suggesting they are almost fully saturated. On the other hand, the saponification numbers are different between the fuels (330 and 233). This implies that C1214 has longer average carbon chain length than C810. For convenience, C810 and C1214 are referred to as “shorter carbon chain biodiesel” and “longer carbon chain biodiesel” in the following sections. The injection pressure was maintained at 100 MPa for both fuels. The injection timing and injection duration were adjusted such that the start of combustion and the total energy input per injection were matched for both fuels.

In-cylinder Pressure and Heat Release Rate

Displacement volume	498 cm ³ (single cylinder)
Bore	83 mm
Stroke	92 mm
Compression ratio	15.5 (geometric)
Wall (coolant) temperature	363 K
Swirl ratio	1.4
Intake air temperature	303 K
Engine speed	1200 rpm
Injector type	Bosch common-rail
Nozzle type	Hydro-grounded, K1.5/0.86
Nozzle hole diameter	134 μm (nominal)
Included angle	150°
Number of nozzle holes	1

Table 1. Engine specifications and operating conditions.

The in-cylinder pressure was measured using a piezoelectric pressure transducer. The pressure traces were ensemble-average over 15 firing cycles, which was then used to derive the apparent heat release (aHRR). The aHRR traces were used to evaluate the in-cylinder conditions and to help identify the combustion phase at the imaging timing.

Planar Laser Imaging and Image Presentation

Figure 1(a) illustrates the engine and laser imaging setup. A horizontal laser sheet was inserted into the engine cylinder through a quartz liner window. The PLIF and PLII as well as the natural chemiluminescence signals are collected through the bowl window and a 45° mirror using an ICCD camera with UV-enhanced lens and corresponding filters. Figure 1(b) shows the laser sheet coverage within the bowl area. The jet of interest was aimed at 2 o'clock direction and two horizontal laser planes at 7 and 9 mm below the cylinder head. An example of OH-PLIF image taken at 7 mm plane is presented with the boundary of bowl window overlaid by a red circle. The corresponding imaging timings are denoted in crank angle degrees after top dead centre (° aTDC) and after the end of injection (° aEOI). Note that for each diagnostic technique, only one laser image was taken during every fired cycle, at each selected crank angle location. Subsequently, one representative image was selected from a 15-image set using a two-dimensional correlation coefficient calculation for interpretation and discussion, similar to [6]. Detailed explanation for this selection method is found in our previous work [7].

Planar Laser-Induced Fluorescence of OH (OH-PLIF) and OH* Chemiluminescence

The OH radical is a well-accepted marker of high-temperature reaction which can be visualised using a PLIF technique [6, 7]. The commonly used excitation wavelength is 284 nm with the resulting fluorescence emissions in the 308–320 nm range [6]. In this study, a Rhodamine-6G-filled dye laser pumped by a frequency doubled Nd:YAG laser beam (532 nm) was used to achieve the desired OH-PLIF excitation wavelength of 284 nm [7]. The laser beam was then shaped into a 300 μm thick and 35 mm wide sheet using the sheet making optics (figure 1). Due to the potential interference from the fluorescence signal of fuel molecules and polycyclic aromatic hydrocarbons (PAH) as well as

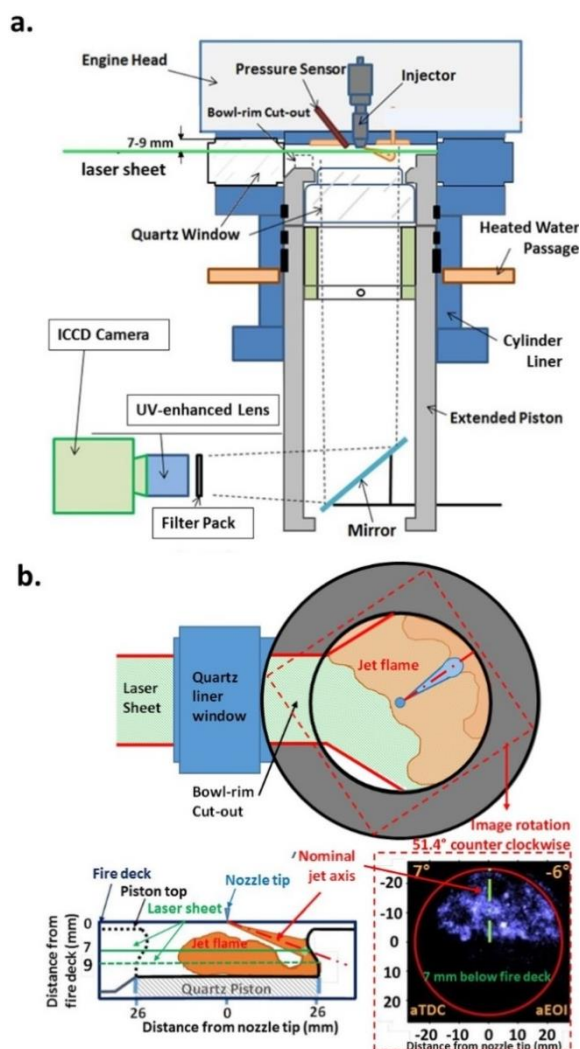


Figure 1. (a) Schematic diagram of the optical diesel engine and laser-based imaging diagnostics setup and (b) illustration of the laser sheets with respect to the piston bowl and the fuel jet in the side view (top) and side view (bottom-left). Also shown on the bottom right is an online PLIF image of longer carbon chain biodiesel fuel obtained at 7 mm below the fire deck.

the incandescence of soot, PLIF imaging was conducted with both laser wavelength tune on (284 nm) and off (283.9 nm) the OH absorption line. A comparison between online and offline OH-PLIF signal were used to verify whether the signal is the due to OH or other interference sources [6]. The filters used for OH-PLIF imaging consist of a 300 nm band-pass filter (40 nm FWHM) and a WG-305 glass filter to reject the scattered laser light. The laser fluence for PLIF imaging was estimated at 0.176 J/cm² before entering the liner window. The camera gate and gain were set at 100 ns and 90%, respectively.

Additionally, electronically excited OH (OH*) radicals were imaged to identify the high-temperature reaction zones during early premixed combustion phase. The imaging was conducted with the same optical filter setup as OH-PLIF imaging (i.e. 300 nm band-pass filter) with a longer exposure of 70 μs and gain of 60%.

Planar laser-induced Incandescence of Soot (PLII)

The fundamental 1064 nm output from the Nd:YAG laser was used for PLII imaging. This wave length was selected to avoid interferences from fluorescence of PAH species [8]. The laser fluence was estimated at 0.72 J/cm² before the liner window. This

Fuel	C810 (Shorter carbon chain)	C1214 (Longer carbon chain)
Fatty acid profile (wt%)		
Caprylic, C8:0	52.16	-
Capric, C10:0	46.38	0.17
Lauric, C12:0	1.38	47.8
Miristic, C14:0	-	18.89
Palmitic, C16:0	-	10.19
Stearic, C18:0	-	2.55
Oleic, C18:1 cis	-	18.53
Linoleic, C18:2	-	1.76
Arachidic, C20:0	-	0.08
Behenic, C22:0	-	0.03
Fuel properties		
Oxygen content (wt%)	18.76	13.38
Iodine value	1.0 max	8
Saponification number	330	233
Relative density @293 K (kg/m ³)	0.877	0.871
Calorific value (MJ/kg)	35.35	38.66
Cetane number	42	69.8
Fuel injection conditions		
Injection pressure (MPa)	100	100
Start of injection (°CA bTDC)	11	4
End of injection (°CA aTDC)	6.8	13
Injection duration (ms)	2.45	2.34

Table 2. Fuel composition, properties and injection conditions

fluence level is well beyond the sub-limitation threshold of soot particles and therefore mitigating possible impacts on LII signal due to the laser shot-to-shot variations and potential beam attenuation [8]. A 430 nm band-pass filter (10 nm FWHM) was used to collect broadband incandescence signal (< 500 nm). A 450 nm short-pass filter was also used to block potential fluorescence signals from gaseous species (e.g. C_2) as well as broadband flame luminosity within the collection range [8]. A 50-ns camera gate and 70% gain were used.

Results and Discussion

In-cylinder Pressure and Apparent Heat Release Rate

Figure 2 shows the 15-cycle-averaged in-cylinder pressure (top) for motored (solid curve) and fired modes (dotted curves). Showing at the bottom are the corresponding aHRR traces for fired mode. It can be seen that the rapid raising of in-cylinder pressure and aHRR occurred at around 4°CA aTDC for both fuels, suggesting similar timing of combustion onset. This was intended to mitigate the impact of in-cylinder conditions on high-temperature reaction and soot formation. The ignition delay is shorter for the longer carbon chain biodiesel, which is consistent with its higher cetane number listed in table 2 and previous studies (e.g. [3]). As a result, longer carbon chain biodiesel had less pre-mixing evidenced by lower peak pressure, aHRR and a more pronouncing mixing-controlled combustion phase.

Development of High-Temperature Reaction

Figure 3 shows the OH^* chemiluminescence images pseudo coloured in cyan and combined online (light blue)/offline (yellow) OH-PLIF images. The combined images are shown for both 7 mm (middle) and 9 mm (bottom) laser planes. The imaging timing (5- 7°CA aTDC) covers the premixed combustion phase. The images show that the OH^* signals start to grow near the jet axis and off the bowl wall for both fuels. However, the signal for the longer carbon chain biodiesel is observed closer to the bowl wall, which is not found for the shorter carbon chain biodiesel. The OH-PLIF signals for the shorter carbon chain biodiesel show much larger coverage than the corresponding OH^* signal at early timing. The mismatching between OH^* and OH-PLIF signals suggests interference from other sources was significant. Indeed, the overlapping between online and offline OH-PLIF signals are

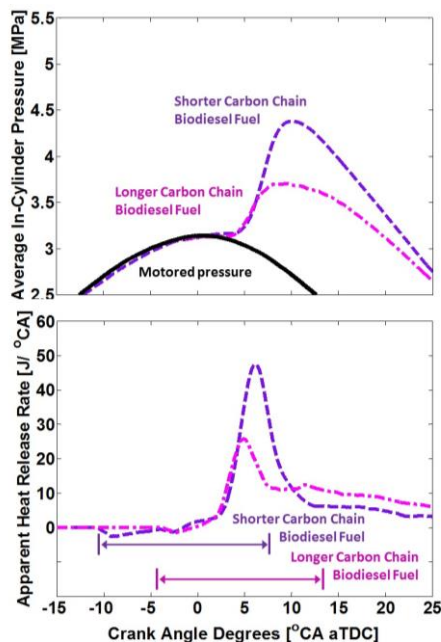


Figure 2. Averaged in-cylinder pressure (top) and the apparent heat release rate (aHRR) traces (bottom).

observed at 5°CA aTDC evidenced by high intensity white coloured regions at the leading edge of penetrating wall-jet head and jet-wall impingement zone. As discussed in our previous study, the OH-PLIF signal outside of the OH^* signal region is predominantly due to fluorescence from the fuel under UV excitation [7]. The interference subsides significantly after the end of injection at 7°CA aTDC as OH-PLIF signals disappear in the jet-wall impingement zone for 7 mm laser plane. However, the yellow offline OH-PLIF signal is still apparent in the near-wall region at 9 mm plane, suggesting the persistence of fuel-rich mixtures. By contrast, the longer carbon chain biodiesel shows much lower interference from fuel fluorescence which is only apparent at the jet-wall impingement point. The OH-PLIF signal is consistent with the OH^* signal and shows larger coverage at the lower laser plane (9 mm). This suggests that the high temperature reaction started to develop in the penetrating wall-jet head after the fuel jet impingement on the bowl wall, which continued to travel towards the other side of the bowl. Therefore, the observed difference in spatial distribution of OH^* and OH-PLIF signals suggests that the high temperature reaction occurs further upstream of the wall-impinging fuel jet for the longer carbon chain biodiesel due to shorter ignition delay.

Soot Formation, Development and Oxidation

Figure 4 shows combined OH-PLIF and PLII (red) signals at 7 and 9 mm laser planes for both biodiesel fuels. The LII signals suggest that soot formation occurred at roughly the same timing (9°CA aTDC) for both fuels, at the end of premixed combustion phase (figure 2). The soot formation starts to occur at the jet-wall impingement region for the shorter carbon chain biodiesel where the fuel-rich mixture is presented [9]. The LII signal grows rapidly at 11°CA aTDC and interacts with the OH region near the centre

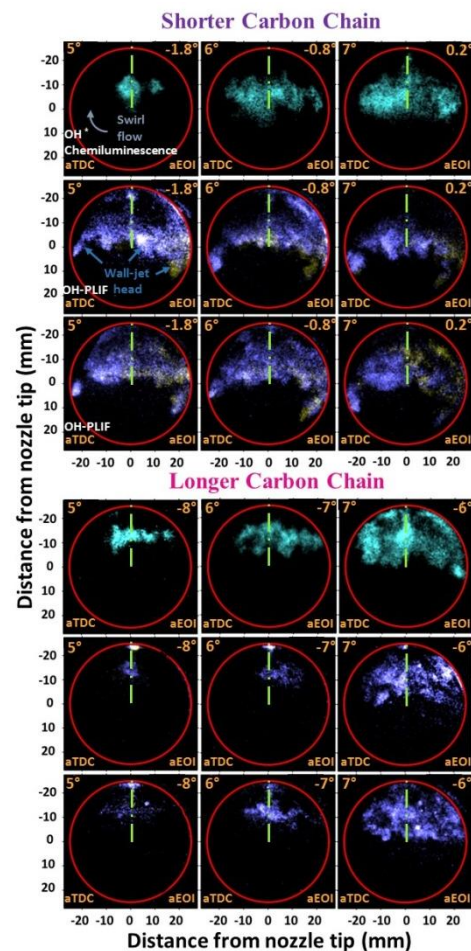


Figure 3. OH^* chemiluminescence (top row) and signals of combined online (blue) and offline (yellow) OH-PLIF at 7mm (middle row) and 9 mm (bottom row) below the cylinder head.

of the bowl. At 13°C aTDC, the simultaneous disappearance of OH-PLIF and LII signal are observed around the jet-wall impingement region. It suggests that the OH radicals in those regions were consumed for soot oxidation [7]. The remaining soot pockets continue to travel along the bowl-wall while shrinking in size, which suggests continuous soot oxidation. By contrast, the longer carbon chain biodiesel shows additional soot formation in the wall-jet head region. This is due to a more fuel-rich mixture condition as the result of less premixing (figure 2) and lower fuel oxygen content (table 2). In addition, as a larger fraction of the injected fuel was burnt during the mixing-controlled burn phase for the longer carbon chain biodiesel, the soot pockets grew faster. Although soot oxidation is evident by the reduced soot region at 15°C aTDC, the remaining soot level at 17°C aTDC is much higher for the longer carbon chain biodiesel. The limited soot oxidation is likely due to lower fuel oxygen content as well as relatively less interactive distribution of OH and soot.

Conclusion

The imaging of OH-PLIF, OH* chemiluminescence, and PLII were performed for two biodiesel fuels with different carbon chain lengths in an optical diesel engine. The results show that, with a fixed start of combustion and total energy input, increasing the biodiesel carbon chain length leads to a shorter ignition delay. This causes the OH to develop closer to the bowl-wall, where the jet-wall impingement occurs. The longer carbon chain biodiesel also shows overall higher LII signals due to increased soot formation and limited OH-induced oxidation.

Acknowledgments

Experiments were conducted at the UNSW Engine Research Laboratory. Support for this research was provided in part by the Australian Research Council. Masri and Pham are supported by a NPRP award [NPRP 7-036-2-018] from the Qatar National Research Fund (a member of The Qatar Foundation).

References

- [1] Lapuerta, M. & Fernández J.R., Effect of biodiesel fuels on diesel engine emissions, *Prog. Energ. Combust.*,**34**, 2008, 198-223.
- [2] Johansson, M., Yang, J., Ochoterena, R., Gjirja, S. & Denbratt, I., NOx and soot emissions trends for RME, SME and PME fuels using engine and spray experiments in combination with simulations, *Fuel*,**106**, 2013, 293-302.
- [3] Schönborn, A., Ladommatos, N., Williams, J., Allan, R. & Rogerson, J., The influence of molecular structure of fatty acid monoalkyl esters on diesel combustion, *Combust. Flame*,**156**, 2009, 1396-1412.
- [4] Pham, P.X., Bodisco, T.A., Stevanovic, S., Raham, M.D., Wang, H., Ristovski, Z.D., Brown, R.J. & Marsri, A.R., Engine performance characteristics for biodiesels of different degrees of saturation and carbon chain lengths, *SAE Int. J. Fuels Lubr.*,**6**, 2013, 188-198.
- [5] Pasunurthi, S.S., Hawkes, E.R., Joelsson, T., Rusly, A.M., Kook, S., Lucchini, T. & D'Errico, G., Numerical study of a diesel engine under motored and combustion conditions, in *Proceedings of the 9th Asia-Pacific Conference on Combustion*, 2013.
- [6] Musculus, M.P.B., Multiple simultaneous optical diagnostic imaging of early-injection low-temperature combustion in a heavy-duty diesel engine, SAE Paper 2006-01-0079, 2006.
- [7] Le, M.K., Zhang, R., Rao, L., Kook, S. & Hawkes, E.R., The development of hydroxyl and soot in a methyl decanoate-fuelled automotive-size optical diesel engine, *Fuel*,**166**, 2016, 320-332.
- [8] Michelsen, H.A., Schulz, C., Smallwood, G.J. & Will, S., Laser-induced incandescence: Particulate diagnostics for combustion, atmospheric, and industrial applications, *Prog. Energ. Combust.*,**51**, 2015, 2-48.
- [9] Bruneaux, G., Combustion structure of free and wall-impinging diesel jets by simultaneous laser-induced fluorescence of formaldehyde, poly-aromatic hydrocarbons, and hydroxides, *Int. J. Engine Res.*,**9**, 2008, 249-265.

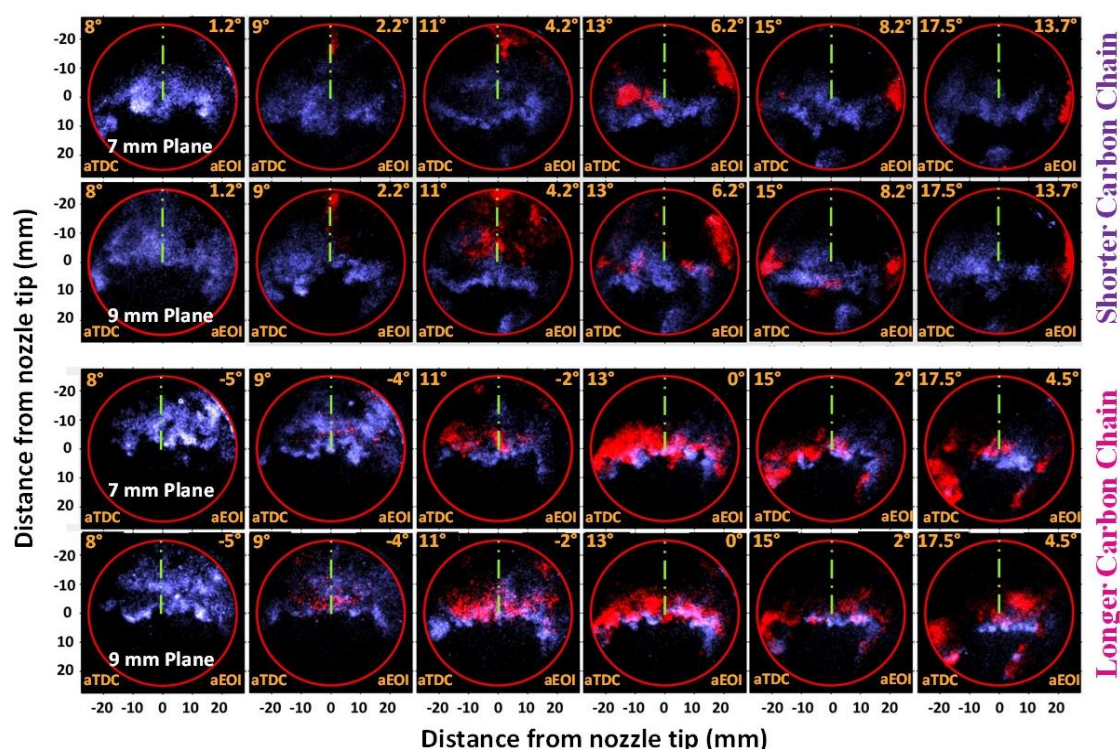


Figure 4. The combined images of online OH-PLIF (blue) and PLII (red) signals between 8 °CA and 17.5 °CA aTDC for biodiesel fuels with different carbon chain lengths at both 7 mm and 9 mm plane below the fire deck.